Research on Design Methodology and Finite Element Analysis of Inner Cores for Multi-Level Energy Dissipation and Self-Centering BRBs — Part I: Aluminum Alloy Core with ECC Encasement

Suokun Chen[1], Wei Zhang[2], Xiaomin Huang[3*], Fang Wei[4], Weibing Xu[4], Hang Sun[5]

[1] China Aluminum Southwest Construction Investment Co., Ltd, Kunming, Yunnan, China
[2] China Nonferrous Metals Processing Technology, Co., Ltd, Beijing, China
[3]Kunming University of Science and Technology, Kunming, Yunnan, China
[4]Beijing University of Technology, Beijing, China
[5] Harbin Institute of Technology, Harbin, China

*Corresponding Author: Xiaomin Huang.
Email: huangxm.yu@kust.edu.cn

Abstract. This paper proposes an innovative inner core for buckling-restrained braces with multi-mechanism energy dissipation and self-centering capabilities, referred to as Aluminum-ECC-Self-Centering Conical Taper (ALECCYT) inner core. Through theoretical deduction, an initial design methodology for the horizontal and vertical (structural) parameters of the outer ECC-wrapped aluminum (ALECC) inner core is presented. Based on this methodology, three ALECC braces with different tonnage capacities are designed. Subsequently, a finite element simulation analysis is conducted to qualitatively and quantitatively analyze the failure modes, hysteretic performance, and related indicators of the specimens, thereby verifying the effectiveness of the design methodology and the superiority of the ALECC inner core structure. The results indicate that the failure mode of the ALECC inner core specimens is the yield failure of the aluminum rod in the middle section, with ECC fully exerting its role in buckling prevention and energy dissipation. Compared to aluminum alloy braces, the ALECC inner core exhibits significantly improved bearing capacity and energy dissipation capacity, as well as enhanced hysteretic performance. The proposed preliminary design methodology for the ALECC inner core demonstrates good applicability.

Keywords: buckling-restrained brace inner core; multi-level energy dissipation; ECC; aluminum alloy; design methodology; hysteretic performance

1 Introduction

Buckling-restrained braces (BRBs) exhibit excellent energy dissipation performance and stability, capable of bearing part of the structural load. They maintain elasticity under normal use and minor seismic activities, providing lateral stiffness for the

G. Zhao et al. (eds.), *Proceedings of the 2024 7th International Symposium on Traffic Transportation and Civil Architecture (ISTTCA 2024)*, Advances in Engineering Research 241,
https://doi.org/10.2991/978-94-6463-514-0_50

structure. Under significant seismic events, BRBs yield and dissipate energy prior to the structure, widely applied in vibration control for building structures [1, 2]. The BRB typically consists of an inner core, an outer sleeve, and unbonded materials in the lateral direction [3].

The mechanical properties of the inner core are crucial for the vibration control effect. However, current inner core designs face multiple limitations, including the shape of the inner core's cross-section, material types, energy dissipation components, and functional applications. Existing cross-section shapes mainly include I-shaped [4], cruciform [5], H-shaped [6-8], T-shaped [9], and channel-shaped. Inner core materials are mostly high-yield-strength steel [10-12], which is not efficient in energy dissipation during minor seismic events. Additionally, current energy dissipation components lack multi-level dissipation and self-centering mechanisms.

To address these issues, this paper proposes an aluminum-ECC-self-centering conical taper (ALECCYT) inner core with multi-mechanism energy dissipation and self-centering functions. The design methodology and hysteretic performance of the outer ECC-wrapped aluminum (ALECC) inner core are explored through theoretical analysis and finite element simulation.

2 ALECCYT Inner Core Design Concept and Structure

2.1 Design Concept

Existing BRBs often use steel as the inner core, which cannot promptly dissipate energy during minor seismic events to protect the structure. Aluminum alloy, with a lower elastic modulus than steel, good ductility, and a low yield point, can be used as an alternative material. However, using aluminum alloy alone as the inner core can easily lead to buckling, severely affecting its mechanical performance. To improve its compressive stability, high-ductility engineered cementitious composite (ECC) can be cast around the aluminum alloy rod. ECC not only limits the buckling of the aluminum alloy rod but also has excellent energy dissipation due to its high toughness and tensile properties, enhancing the energy dissipation capability of the BRB. Figure 1 shows the stress deformation cloud diagram of the aluminum alloy rod with ECC encasement during failure.

The figure indicates that ECC effectively improves the buckling resistance of the aluminum alloy rod. However, due to the significant difference in ultimate strain between the two materials, ECC may fail prematurely while the aluminum alloy rod remains undamaged, resulting in poor synergy. Figure 2(a) shows the hysteretic curve of the aluminum alloy rod with full-length ECC encasement. Figure 2(b) shows that the compressive bearing capacity of the aluminum alloy rod with ECC encasement significantly improves, and overall buckling is mitigated. However, due to the lower tensile strength of ECC compared to its compressive strength, the tensile bearing capacity of the aluminum alloy rod with ECC encasement is significantly lower than its compressive capacity. The deformation capacity of the aluminum alloy rod with ECC encasement is also smaller than that of the aluminum alloy rod alone due to the lower ductility of ECC compared to metal materials.

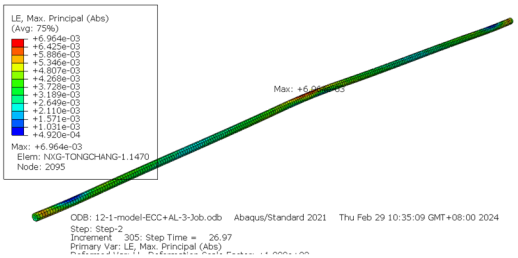

(a) Aluminum rod

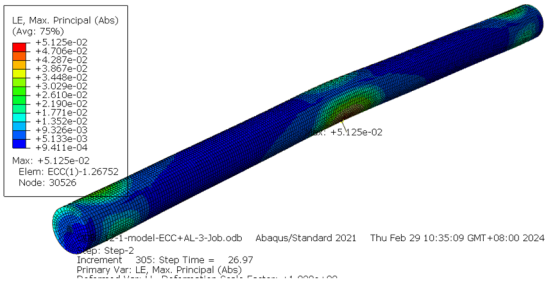

(b) ECC shell

Fig. 1. Stress-strain cloud chart of fully cast ECC aluminum alloy rod

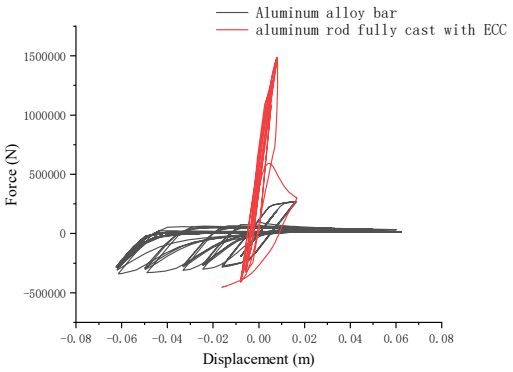

Fig. 2. Hysteresis loop of reciprocating loading on AlECC core

To achieve both buckling resistance and symmetrical tension-compression behavior, ECC is applied to the ends of the aluminum alloy rod, causing the middle section of the aluminum rod to yield first, followed by ECC failure. The structure is illustrated in Figure 3. Figure 4 shows the hysteretic curve of a typical ALECC inner core (designed bearing capacity of 30 tons, length of 5 meters) under cyclic loading. It is observed that the buckling of the inner core is significantly improved, with improved symmetry in tensile and compressive bearing capacities and enhanced deformation capacity.

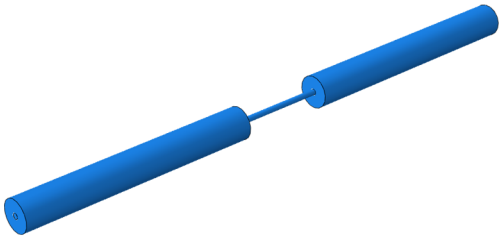

Fig. 3. Diagram of internal structure of ALECC

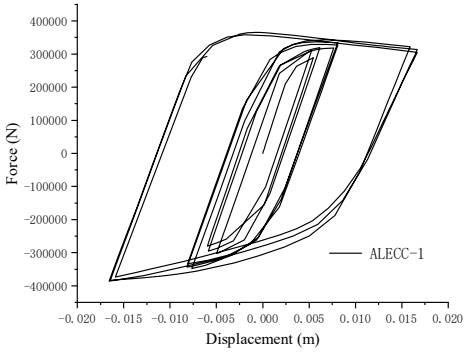

Fig. 4. Hysteresis loop of aluminum alloy rod with partial cast ECC

While the ALECC inner core improves the buckling issue of the aluminum alloy rod, its residual deformation is considerable after loading. To reduce residual strain and achieve some self-centering capability, scholars often use prestressed steel tendons to provide self-centering ability for BRBs [13-16]. However, BRBs using prestressed tendons for self-centering have limited plastic deformation capacity. Therefore, this paper designs a self-centering system using shape memory alloy (SMA), which has a large elastic deformation capacity. The self-centering system unit is shown in Figure 5, with a frustum shape connected in series around the ALECC inner core, forming the self-centering frustum device (YT) as illustrated in Figure 6. This structure allows all three materials to bear deformation, with the SMA rods providing secondary energy dissipation and restoring force, and the steel rings and CFRP tendons supplementing the energy dissipation capacity.

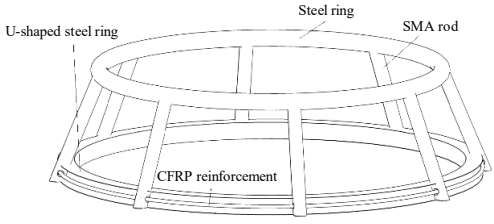

Fig. 5. Self-resetting conical unit

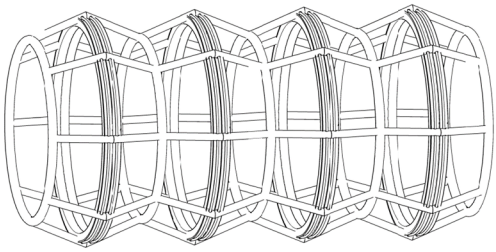

Fig. 6. Self-resetting conical device

Figure 7 shows the stress deformation cloud diagram of the ALECCYT inner core under maximum compressive bearing capacity during cyclic loading. It is observed that the middle section of the aluminum rod enters a buckling state, reaching yield strength, while the YT remains unbuckled during compression. Figure 8 compares the hysteretic curves of the ALECC and ALECCYT inner cores. The ALECCYT inner core exhibits enhanced energy dissipation and self-centering capabilities, with the SMA starting to phase transform after the aluminum rod buckles, providing additional energy dissipation and self-centering. The hysteretic curves show distinct flag-shaped characteristics, indicating significant improvements in energy dissipation capacity, and the residual displacement is reduced by 91.07% compared to the ALECC inner core.

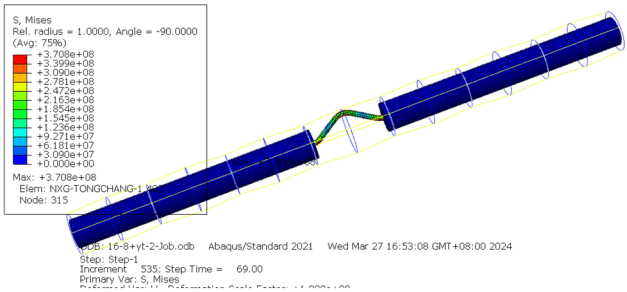

Fig. 7. Stress-strain cloud chart of aluminum-ECC-self-resetting conical unit composite core rod

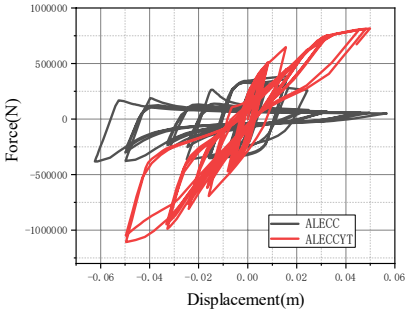

Fig. 8. Comparison of hysteresis loops between ALECC core `and ALECCYT core

This new ALECCYT inner core for buckling-restrained braces has the following advantages: efficient energy dissipation capability to protect the main structure during minor seismic events, use of low-yield-point aluminum alloy and ECC as energy dissipation materials to restrict aluminum rod buckling, excellent energy dissipation capacity, multi-level energy dissipation to increase energy dissipation safety reserves, and self-centering capability to significantly reduce residual displacement.

2.2 Structure

Based on the above design concept, Figure 9 shows the structural schematic of the ALECCYT inner core. The primary energy dissipation inner core is composed of A5083-H111 aluminum alloy and ECC with a compressive strength of 40 MPa. The YT's steel rings are made of Q235 steel, the SMA is Ti-50.8at%Ni, and the CFRP rings are made according to Hu Qidong's specifications [17]. The aluminum rod has crescent ribs on its surface for mechanical interlock and chemical bonding with ECC. The YT components are welded and tied together, mounted around the ALECC inner core, and connected to the end plates.

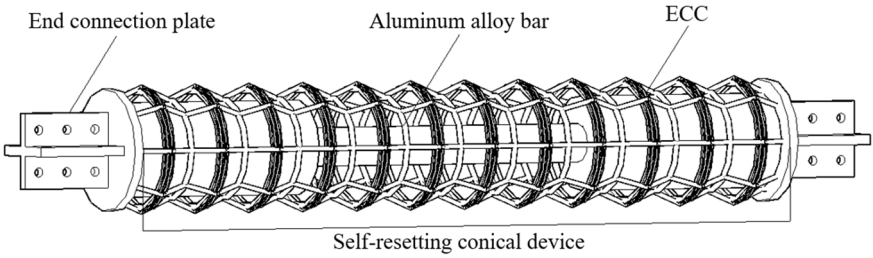

Fig. 9. Schematic diagram of the structure of aluminum-ECC-self-resetting conical unit composite core rod

3 Simplified Design Methodology for ALECC Inner Core

The design parameters of the ALECC inner core significantly influence its failure mode. Therefore, this section first designs the horizontal and vertical dimensions of the ALECC inner core based on the preset failure mode. The failure mode is set to have the middle aluminum rod yield before ECC fails, ensuring that the ultimate stress of ECC is not reached when the aluminum rod yields, avoiding instability failure.

3.1 Horizontal Design

Firstly, the horizontal dimensions are designed based on the failure mode where the middle aluminum rod yields before the ECC fails. For the aluminum rod with ECC encasement, as shown in Figure 10, segments AB and CD are aluminum rods with ECC encasement, and segment BC is the aluminum rod only. To ensure ECC supplements

the bearing capacity of the aluminum rod and fully utilizes its tensile and compressive energy dissipation, the failure mode is preset to have the aluminum rod yield before ECC fails, thereby maximizing ECC's energy dissipation capacity. The total deformation consists of two parts, as shown in Formula (1).

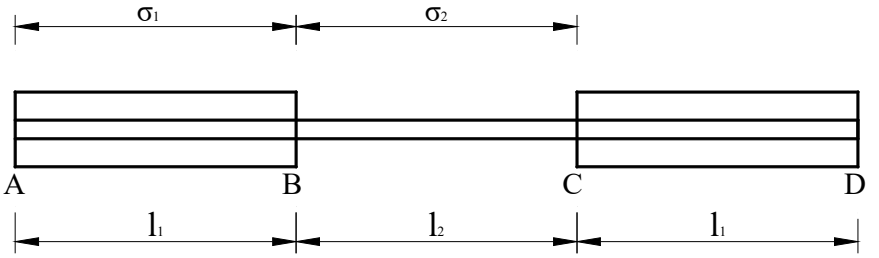

Fig. 10. Diagram of Al+ECC construction

$$2\frac{\sigma_{AB}}{E_{AB}}l_{AB} + \frac{\sigma_{BC}}{E_{BC}}l_{BC} = \Delta_l \tag{1}$$

Where:

σ_{AB}, σ_{BC}——stresses in segments AB and BC;
E_{AB}, E_{BC}——equivalent elastic moduli of segments AB and BC;
l_{AB}, l_{BC}——lengths of segments AB and BC.
When the aluminum rod yields, the external force on the rod is:

$$F_y = \sigma_{y2}.A_2 \tag{2}$$

σ_{y2}, A_2——yield strength and cross-sectional area of the aluminum rod.
At this point, the stress in segment AB is:

$$\sigma_{AB} = \frac{F_y}{A_1+A_2} \tag{3}$$

Segment AB is a combination of ECC and aluminum rod, with its elastic modulus:

$$E_{AB} = \frac{E_1A_1+E_2A_2}{A_1+A_2} \tag{4}$$

E_1, A_1——elastic modulus and cross-sectional area of ECC;
E_2, A_2——elastic modulus and cross-sectional area of the aluminum rod.
The stress in segment BC is:

$$\sigma_{BC} = \sigma_{y2} \tag{5}$$

σ_{y2}——elastic modulus of segment BC:
The elastic modulus of segment BC:

$$E_{BC} = E_2 \tag{6}$$

Substituting Formula (2) to (6) into Formula (1), Formula (1) becomes:

$$2\frac{\sigma_{y2}.A_2}{E_1A_1+E_2A_2}l_{AB}+\frac{\sigma_{y2}}{E_2}l_{BC}=\Delta_l \tag{7}$$

$2\frac{\sigma_{y2}.A_2}{E_1A_1+E_2A_2}l_{AB}$ represents the deformation shared by segments AB and CD; $\frac{\sigma_{y2}}{E_2}l_{BC}$ represents the deformation shared by segment BC.

From Formula (7), it can be seen that under a constant total deformation and unchanged other variables, the larger A1 is, the smaller the deformation shared by segments AB and CD, and the larger the deformation shared by segment BC. Thus, the aluminum rod in segment BC is more likely to fail before the ECC. Therefore, the cross-sectional size of ECC is designed based on the principle that the aluminum rod should fail before the ECC. This principle can be interpreted as: when the external force reaches the yield strength of the aluminum rod, the ECC stress has not yet reached its ultimate stress. For the aluminum rod wrapped with ECC at both ends, the external force during failure is as shown in Formula (2), $F_y=\sigma_{y2}\cdot A_2$. The cross-section of segment AB is shown in Figure 11, where rr is the radius of the aluminum rod and RR is the outer diameter of the ECC.

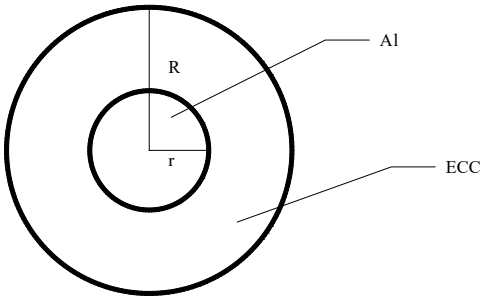

Fig. 11. Schematic diagram of the cross-section construction of ALECC core AB segment

Segment AB consists of ECC and aluminum rod, with the following relationship:

$$F_1+F_2=F_y \tag{8}$$

Where F_1 represents the external force shared by the ECC in segment AB.

$$F_1=\sigma_1.(\pi R^2-\pi r^2) \tag{9}$$

Where F_2 is the external force borne by the ECC in segment AB:

$$F_2=\sigma_2.\pi r^2 \tag{10}$$

σ_1, σ_2——stresses in ECC and aluminum rod in segment AB.
According to the stress-strain relationship:

$$\frac{\sigma_1}{E_1}=\varepsilon_1 \tag{11}$$

$$\frac{\sigma_2}{E_2}=\varepsilon_2 \tag{12}$$

$\varepsilon_1, \varepsilon_2$——strains in ECC and aluminum rod.

Since the deformations of ECC and aluminum rod in segment AB are coordinated:

$$\varepsilon_1 = \varepsilon_2 \tag{13}$$

Substituting Formula (11) and (12) into Formula (13):

$$\frac{\sigma_1}{\sigma_2} = \frac{E_1}{E_2} \tag{14}$$

Combining Formula (2), (8), (9), (10), and (14):

$$\sigma_1 = \frac{E_1 \sigma_{y2} r^2}{(E_2 - E_1) r^2 + E_1 R^2} \tag{15}$$

At this time, the stress in the ECC of segment AB should be less than its tensile ultimate stress (the tensile ultimate stress of ECC is lower than its compressive ultimate stress):

$$\sigma_1 < \sigma_{tu1} \tag{16}$$

σ_{tu1}——tensile ultimate stress of ECC.

Combining Formula (15) and (16), the theoretical formula for horizontal design is obtained as follows:

$$R > r\sqrt{\frac{\sigma_{y2}}{\sigma_{tu1}} - \left(\frac{E_2}{E_1} - 1\right)} \tag{17}$$

3.2 Longitudinal Design

Given the bearing capacity, after determining the cross-sectional area of the rod based on the above derivation, the longitudinal length of the rod should be designed to ensure that the failure mode is yield failure, not buckling failure. Therefore, a stability analysis is required. The classical Euler formula gives the critical buckling force for slender compression members:$P_{cr} = \frac{\pi^2 EI}{(\mu l)^2}$[18,19]. To prevent the brace from undergoing overall buckling failure and ensure yield failure:

$$P_{cr} \geq P_y \tag{18}$$

Where E is the elastic modulus of the rod material, I is the moment of inertia of the rod cross-section, $\mu\mu$ is the effective length factor related to the boundary conditions of the rod, and ll is the actual length of the compression rod. P_y is the yield load of the rod.

Next, the stability of each section of the composite rod is analyzed.

(1) Stability Analysis of the Middle Aluminum Rod Segment

Regardless of whether the constraints at both ends of the ALECC inner core are fixed or hinged, the constraints at both ends of the middle aluminum rod are between fixed and hinged.

1) When the Constraint Condition is Hinged:

$$P_{cr} = \frac{\pi^2 E_2 I_2}{{l_2}^2} \tag{19}$$

To ensure the rod does not fail due to buckling:

$$P_{cr} = \frac{\pi^2 E_2 I_2}{{l_2}^2} \geq \sigma_{y2}.A_2 = P_y \tag{20}$$

It can be inferred

$$l_2 \leq \sqrt{\frac{\pi^2 E_2 I_2}{\sigma_{y2}.A_2}} \tag{21}$$

2) When the boundary conditions are fixed:

$$P_{cr} = \frac{\pi^2 E_2 I_2}{(0.5 l_2)^2} \tag{22}$$

To ensure the aluminum rod segment does not buckle before yielding, the following condition must be satisfied:

$$P_{cr} = \frac{\pi^2 E_2 I_2}{(0.5 l_2)^2} \geq \sigma_{y2}.A_2 = P_y \tag{23}$$

It can be inferred

$$l_2 \leq 2\sqrt{\frac{\pi^2 E_2 I_2}{\sigma_{y2}.A_2}} \tag{24}$$

To ensure the design results are conservative, the longitudinal length of the middle aluminum rod should be designed based on the calculation results for the case when the boundary conditions are hinged.

(2) Stability Analysis of the ECC-Aluminum Rod Composite Segment

Similarly, the boundary conditions at both ends of the ECC-aluminum composite segment lie between fixed and hinged supports.

1) When the boundary conditions are hinged

According to the study by Ouyang et al. [3], the critical buckling force formula for composite members is

$$P_{cr} = \frac{\pi^2 (E_1 I_1 + E_2 I_2)}{{l_1}^2} \tag{25}$$

To prevent buckling failure, there should be

$$P_{cr} = \frac{\pi^2 (E_1 I_1 + E_2 I_2)}{{l_1}^2} \geq \sigma_{y2}.A_2 = P_y \tag{26}$$

It can be inferred

$$l_1 \leq \sqrt{\frac{\pi^2 (E_1 I_1 + E_2 I_2)}{\sigma_{y2}.A_2}} \tag{27}$$

2) When the boundary conditions are fixed

$$P_{cr} = \frac{\pi^2(E_1I_1+E_2I_2)}{(0.5l_1)^2} \tag{28}$$

To prevent buckling failure, there should be

$$P_{cr} = \frac{\pi^2(E_1I_1+E_2I_2)}{(0.5l_1)^2} \geq \sigma_{y2}.A_2 = P_y \tag{29}$$

It can be inferred

$$l_1 \leq 2\sqrt{\frac{\pi^2(E_1I_1+E_2I_2)}{\sigma_{y2}.A_2}} \tag{30}$$

To ensure a more conservative design result, the longitudinal length of the ECC-aluminum composite segment in this area should also be designed based on the calculation results under hinged boundary conditions.

3.3 Design process

According to the above inference, the design process for the ALECC core is illustrated in Figure 12.

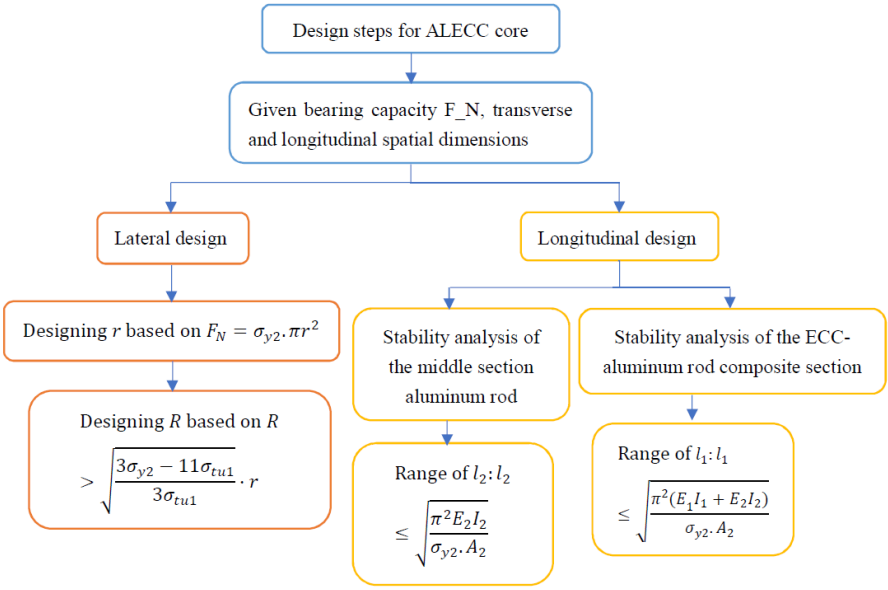

Fig. 12. Flowchart of ALECC core design

3.4 Prototype design

To verify the accuracy of this design method and understand the hysteresis performance of the ALECC core, three different tonnage ALECC cores are designed according to

the above design process, with a longitudinal length of 5m and a lateral width not exceeding 0.5m. Finite element modeling and analysis are conducted. The detailed design information for each specimen is provided in Table 1.

Table 1. Detailed design information of ALECC core specimen

Specimen Number	Design F_N	Calculated r	Value of r	Calculated R>	R	Calculate <	l_2	Calculate <	l_1
ALECC-1	30	0.02485	0.025	0.13622	0.14	0.836	0.8	12.153	2.1
ALECC-2	40	0.0287	0.03	0.16346	0.17	1.003	0.9	14.932	2.05
ALECC-3	50	0.03209	0.033	0.17981	0.18	1.103	1	15.223	2

Note: F_N is in tons; r、R、l_2、l_1 are in meters.

4 Finite element modeling and constitutive validation

The ABAQUS software was used to conduct finite element simulation analysis on the core to validate the design theory. Three-dimensional deformable solid elements were used to model each component of the ALECC core. The ECC and aluminum rods work together and are connected in the finite element model through a 'Tie' constraint relationship. Eight-node linear brick reduced integration elements (C3D8R) were selected to simulate the aluminum alloy rods and ECC. Boundary conditions were set as fully fixed at one end and subjected to axial low-cycle reciprocating displacement loads at the other end. The loading regime was based on the requirements of Dr. Wu Kechuan's thesis, GB 50011-2010 *Code for Seismic Design of Buildings*, and JGJ 99-2015 *Technical Specification for Steel Structures of Tall Buildings*, considering the need for actual axial stiffness measurement and investigating the hysteresis and low-cycle fatigue performance under large strain amplitudes, as shown in Table 2. Low-cycle reciprocating loading was performed at displacement amplitudes of *l*/800, *l*/600, *l*/300, *l*/200, *l*/150, *l*/100, and *l*/80, where *l* is the total length of the anti-buckling support. In the specimens designed in this paper, *l* is 5m. The finite element model of the ALECC core established on the ABAQUS platform is shown in Figure 13.

Table 2. Detailed loading protocol for ALECC core

Loading Mode Control	Loading Level	Strain Amplitude ε_p/%	Displacement Amplitude Δ_p/mm	Number of Cycles *n*/cycles
Displacement Control	1	0.125	$l/800$(0.00625m)	3
	2	0.17	$l/600$(0.00833m)	3
	3	0.33	$l/300$(0.0167m)	3
	4	0.50	$l/200$(0.025m)	3
	5	0.67	$l/150$(0.0333m)	3
	6	1.00	$l/100$(0.05m)	3
	7	1.25	$l/80$(0.0625m)	30/until failure

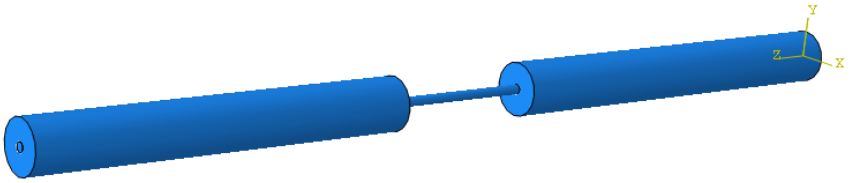

Fig. 13. Finite Element Model Diagram of ALECC Core

The cyclic criterion of aluminum alloy materials includes two characteristics: isotropic strengthening and kinematic hardening [20]. In this study, the Chaboche plasticity constitutive model, which can accurately describe the stress-strain relationship of aluminum alloys, was selected to simulate the stress-strain relationship of aluminum alloys, as shown in Figure 14. The density of aluminum alloy material is 2700 kg/m^3, the elastic modulus is 70 GPa, and the Poisson's ratio is 0.3. Based on experimental data, Jia Bin [20] determined the key material parameters of aluminum alloy materials. In this paper, grade A5083-H111 aluminum alloy was selected, and the material parameters are shown in Table 3. These parameters were input into the plastic-cyclic hardening module provided by the ABAQUS program to define the cyclic constitutive relationship of aluminum alloy materials.

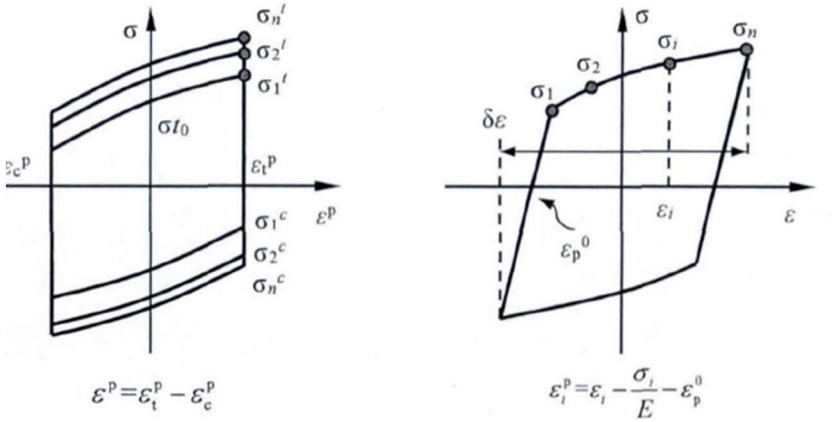

(a) Isotropic Hardening Model (b) Kinematic Hardening Model

Fig. 14. Chaboche plasticity constitutive model

Table 3. Material Parameters of A5083-H111 Aluminum Alloy

Material Grade	$\sigma\|_0$ (MPa)	Q_∞	b	C_1 (MPa)	γ_1	C_2 (MPa)	γ_2	C_3 (MPa)	γ_3	C_4 (MPa)	γ_4
A5083-H111	142.5	84.03	8.98	657	0	2887	359	3485	337	4343	336

To validate the correctness of the aluminum alloy constitutive model, the aluminum alloy standard material test conducted by Li Guochang [21] was simulated using the chosen aluminum alloy constitutive model in this paper, as illustrated in Figure 15. The

stress-strain curve obtained is shown in Figure 16. From Figure 16, it can be observed that the numerical calculation curve trends similarly to the experimental curve. Table 4 provides the yield stress, yield strain, peak stress, ultimate strain, and errors between simulation and experimental specimens. It is noted from Table 4 that, except for a relatively large error in the yield strain, the differences in yield stress, peak stress, and ultimate strain are all less than 5.3%. Therefore, the aluminum alloy constitutive model selected in this paper can be used for finite element simulation of aluminum alloy mechanical properties.

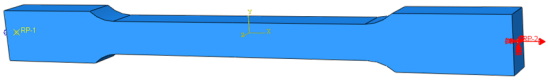

Fig. 15. Finite Element Model of Aluminum Alloy Standard Specimen

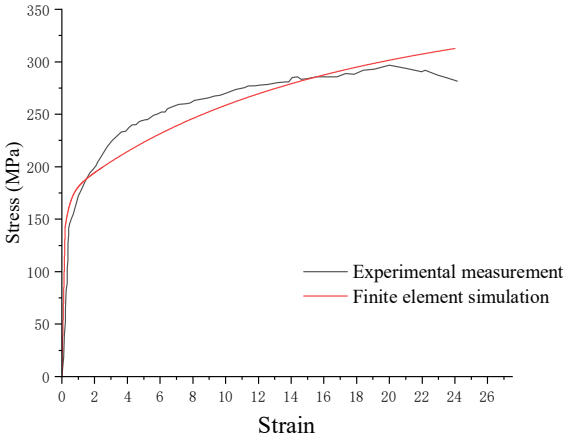

Fig. 16. Validation of Aluminum Alloy Constitutive Model

Table 4. Characteristics Data and Errors of Stress-Strain Curve for Aluminum Alloy

	Yield Strength (MPa)	Yield Strain (%)	Peak Stress (MPa)	Ultimate Strain
Experimental Value	248.0158	5.5212	297	24.1
Simulation Value	247.1166	8.1703	312.6256	24
Error (%)	0.3625	47.9795	5.2611	0.4149

The material constitutive relationship of ECC adopts the model proposed by Yuan [22]. In this model's parameter setting, the density is set to 2100 kg/m^3, the elastic modulus is set to 1.5×10^4 MPa, and the Poisson's ratio is set to 0.17. To validate the

correctness of this ECC constitutive model, the ECC uniaxial tensile test, ECC cubic block compression test, and cylindrical specimen compression test conducted by Cheng Gege [23] were simulated using the ECC constitutive model selected in this paper. The stress-strain curves obtained are shown in Figures 17 and 18. Table 5 provides the yield stress, yield strain, peak stress, ultimate strain, and errors between simulation and experimental specimens. The comparative results indicate that the numerical calculation curve trends similarly to the experimental curve, and the errors in yield stress, yield strain, peak stress, and ultimate strain between simulation and experimental specimens are all below 16.6%. Therefore, the ECC constitutive model selected in this paper can be used for finite element simulation.

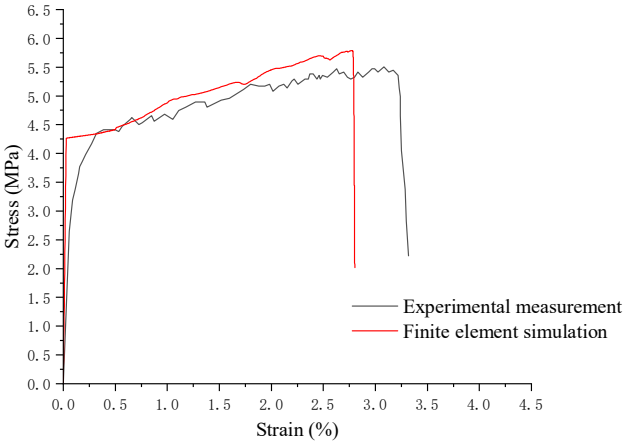

Fig. 17. Validation of ECC Constitutive Model - Tensile Test

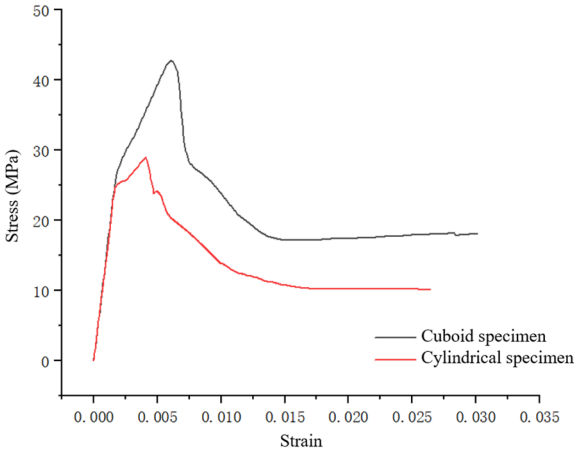

Fig. 18. Validation of ECC Constitutive Model - Compression Test

Table 5. Characteristic Data and Errors of Stress-Strain Curve for ECC in Tension

	Tensile				Compress	
	Yield Strength (MPa)	Yield Strain	Peak Stress (MPa)	Ultimate Strain	Cuboid Compressive Strength	Axial Compressive Strength
Experimental Value	4.5519	0.7756	5.5100	3.2400	41.79	34.6
Simulation Value	4.6140	0.7395	5.7894	2.7930	42.7043	28.8694
Error (%)	1.3642	4.6597	5.0711	13.7973	2.1878	16.5624

5 Analysis of Calculation Results

5.1 Destruction Pattern and Stress State

The stress-strain cloud charts of aluminum rods and ECC at the point of failure for each specimen of ALECC core are illustrated in Figure 19.

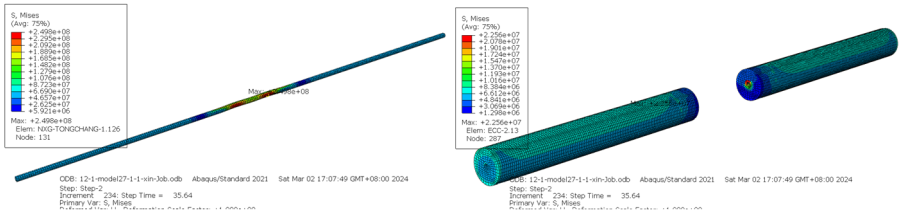

(a) Stress-Strain Cloud Chart of ALECC-1 Aluminum Rod and ECC at Failure

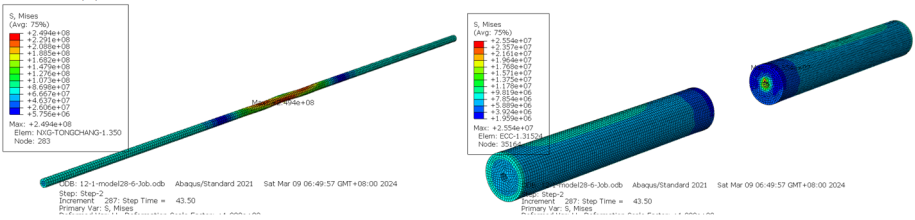

(b) Stress-Strain Cloud Chart of ALECC-2 Aluminum Rod and ECC at Failure

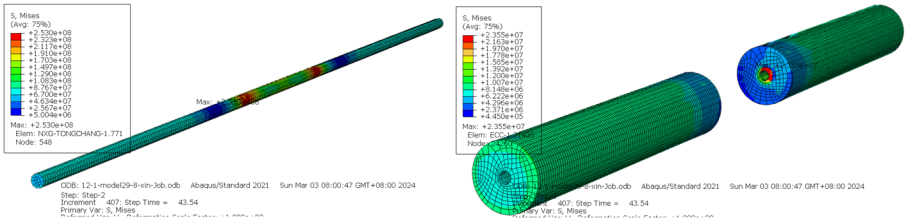

(c) Stress-Strain Cloud Chart of ALECC-3 Aluminum Rod and ECC at Failure

Fig. 19. Stress-Strain Cloud Charts of Aluminum Rod and ECC for Each Specimen

From Figure 19, it can be observed that:

(1) During failure, only a portion of the middle section of the aluminum rods reaches the yield strength, and deformation is concentrated in the middle section of the aluminum rods, without significant buckling. This outcome aligns with the expected results, indicating the correctness of the design method proposed in this chapter.

(2) The overall deformation of ECC is minimal, with significant stress and deformation occurring only near the inner side of the ECC close to the middle section of the aluminum rods. This is because the theoretical derivation assumes uniform stress distribution on the component, with the stress used in the derived formulas being the average stress. However, in actual situations, stress is not uniformly distributed on the component, with the ECC stress near the aluminum rods and the middle section of the aluminum rods being significantly higher than at other locations. Nevertheless, the maximum stress on the ECC still does not exceed its compressive limit strength.

In conclusion, the design method proposed in this paper can achieve the expected failure mode.

5.2 Analysis of Hysteresis Performance

Figure 20 illustrates the hysteresis curves of the entire loading process for each specimen of the ALECC core obtained through finite element analysis.

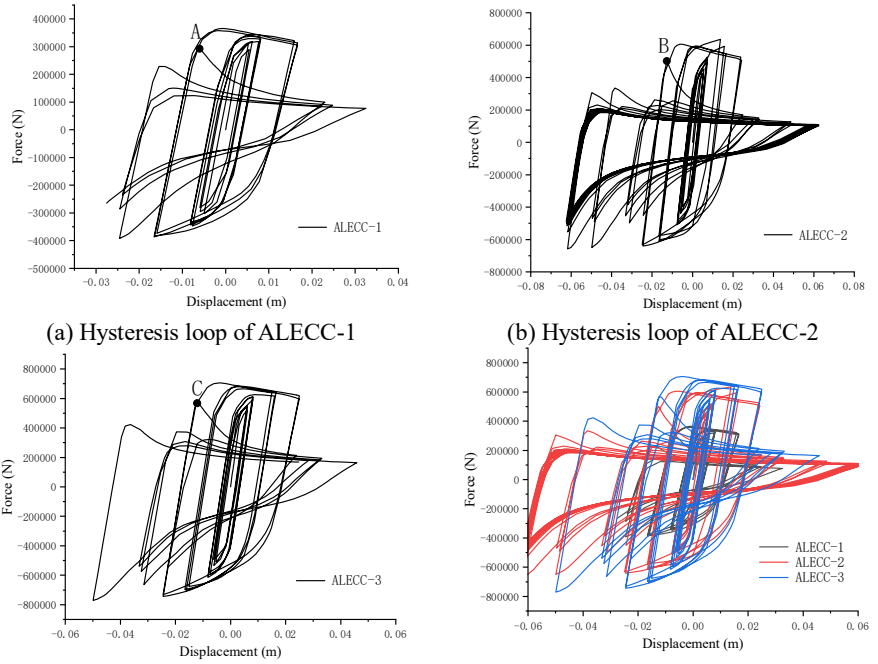

(a) Hysteresis loop of ALECC-1

(b) Hysteresis loop of ALECC-2

(c) Hysteresis loop of ALECC-3

(d) Comparison chart of hysteresis loops for each component

Fig. 20. Hysteresis loops (buckling) of each specimen during the entire finite element loading process of ALECC core

From Figure 20, it can be observed that: ALECC-1 enters a tensile-unloading to compression phase transition at 0.33% strain during the third cycle of loading, corresponding to point A in Figure 20(a) and the stress-strain state shown in Figure 19(a). At this point, the middle section of the aluminum rod enters a buckling state. ALECC-2 transitions from tensile loading to compression at 0.5% strain during the second cycle of loading, corresponding to point B in Figure 20(b) and the stress-strain state shown in Figure 19(b). At this point, the middle section of the aluminum rod undergoes further local or overall buckling. ALECC-3 transitions from tensile loading to compression at 0.5% strain during the second cycle of loading, corresponding to point C in Figure 20(c) and the stress-strain state shown in Figure 19(c). At this point, the middle section of the aluminum rod enters a buckling state. It indicates that all three specimens fail according to the designed failure mode, with buckling occurring after material yielding. Figure 21 illustrates the hysteresis curves of each specimen of the ALECC core before buckling under cyclic displacement loading.

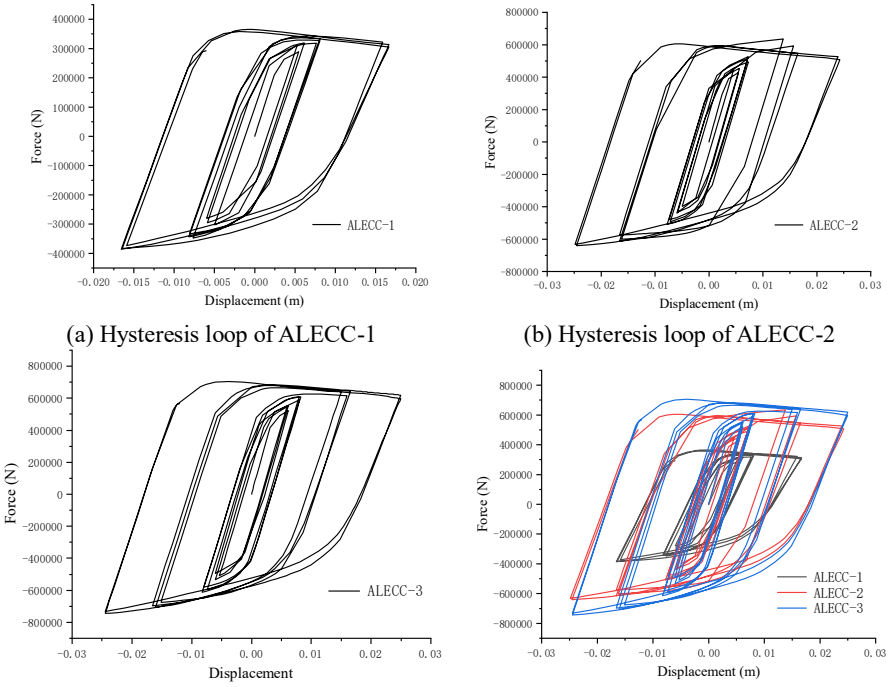

(a) Hysteresis loop of ALECC-1

(b) Hysteresis loop of ALECC-2

(c) Hysteresis loop of ALECC-3

(d) Comparison chart of hysteresis loops for each component

Fig. 21. Hysteresis loops of each specimen of ALECC core before failure

From Figure 21, it can be observed that:

(1) Under the same design load, the energy absorption capacity of the ALECC core (61899.6986 N·m) is 4.43 times that of the aluminum alloy rod (13984.7591N·m), and the maximum compressive load (36.528t) before buckling is 1.38 times that of the aluminum alloy rod (26t), while the maximum tensile load (38.6055t) before buckling is

1.36 times that of the aluminum alloy rod (t). This indicates that pouring ECC around the aluminum alloy core can increase the energy absorption capacity and improve the buckling situation.

(2) The hysteresis curves of each specimen during the tension-compression stage before the yielding of the aluminum alloy material are not completely symmetric, with the compressive load of all three specimens lower than the tensile load. This is mainly due to slight local buckling of the middle section of the aluminum alloy rod before overall buckling.

(3) The ductility of each specimen is similar, but with the increase in design load, the peak value of the hysteresis curve gradually increases, leading to a significant improvement in energy absorption capacity.

5.3 Analysis of Hysteresis Performance Indicators

Combining with the evaluation criteria for hysteresis performance of BRBs [24], an analysis of the hysteresis performance of the ALECC core was conducted, and relevant performance indicators extracted from the loading process of the specimens are presented in Table 6.

Table 6. Hysteresis Performance Indicators of ALECC Core Specimens

	Theoretical Value of K_{eq}	Finite Element Calculated Value of K_{eq}	Tension-compression Unbalance Coefficient β
ALECC-1	1.011×10^8	8.715×10^7	0.9462
ALECC-2	1.379×10^8	1.214×10^8	0.9924
ALECC-3	1.537×10^8	1.352×10^8	0.9489

From Table 6, it can be observed that the theoretical values of equivalent elastic stiffness are slightly higher than the values calculated by finite element analysis, but the error between the finite element analysis values and the theoretical values does not exceed 14%. This discrepancy is due to the theoretical calculation considering the stiffness under ideal loading conditions, whereas in reality, it is difficult for the specimens to be completely in axial tension-compression state. The tension-compression imbalance coefficients of all specimens are less than 1.3, meeting the requirements of the specifications. The tension-compression imbalance coefficient is less than 1, as slight local instability occurs when the specimens are under compression in the later stage of loading.

Figures 22 to 24 respectively depict the distribution of energy coefficient, energy ratio, and equivalent viscous damping ratio of the three specimens under various levels of axial displacement amplitudes before buckling. From Figure 22, it can be observed that the energy coefficients of the three specimens are similar, increasing with the increase of axial displacement amplitude, and reaching a stable trend with a decrease in growth rate in the later stage of loading. The maximum energy coefficients of the three specimens are 2.58, 2.75, and 2.73, respectively. Figure 23 shows that the energy ratios of the three specimens are similar, with a trend of increasing with the increase of axial displacement amplitude similar to that of the energy coefficients. The maximum energy

ratios of the three specimens are 0.65, 0.69, and 0.68, respectively. Figure 24 indicates that the equivalent viscous damping ratios of the three specimens are similar, showing a trend of increasing with the increase of axial displacement amplitude similar to that of the energy coefficients. The maximum equivalent viscous damping ratios of the three specimens are 41.06%, 43.76%, and 43.41%, respectively.

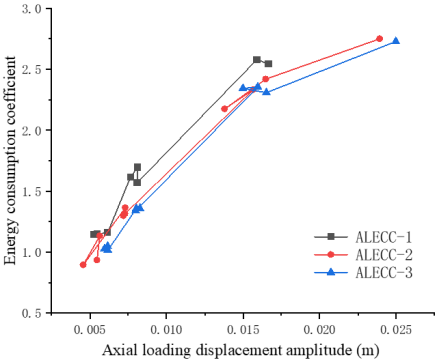

Fig. 22. Distribution chart of damping coefficients

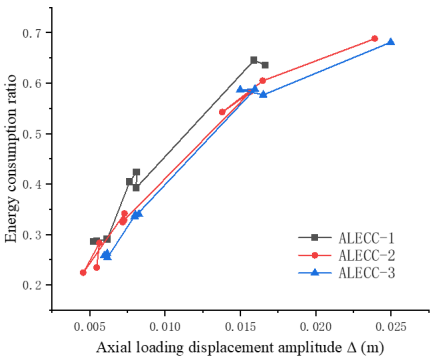

Fig. 23. Distribution chart of energy dissipation ratios

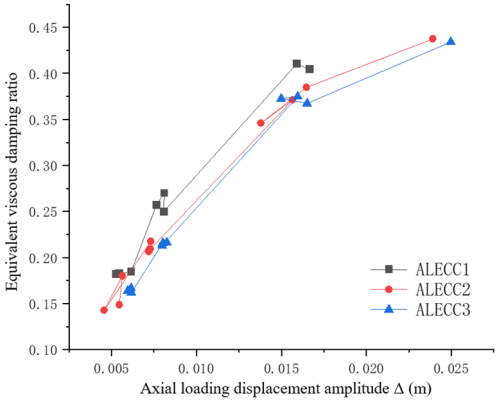

Fig. 24. Distribution chart of equivalent viscous damping ratios

6 Conclusion

The paper introduces a novel aluminum-ECC-self-resetting cone combination (ALECCYT) core designed for anti-buckling support, which possesses multi-mechanism energy dissipation and self-restoring capabilities. Through theoretical analysis and finite element simulation, the design method and hysteresis performance of the ALECC core are investigated, validating the effectiveness of the design method and the

superiority of the ALECC core structure. The main conclusions of the study are as follows:

(1) ALECCYT core, a core designed for anti-buckling support with multi-level energy dissipation and self-resetting functions, is proposed. The design concept and construction form of the ALECCYT core are elaborated, and both lateral and longitudinal design methods of the ALECC core are provided based on the predetermined failure mode.

(2) The ALECC core, designed using the proposed design method, exhibits overall buckling of the middle section of the aluminum rod after material failure, with the failure mode of the specimen being material yield failure. Material failure of the aluminum alloy occurs before that of ECC, showcasing the full utilization of ECC material in preventing buckling and dissipating energy.

(3) Under the same design load, the ALECC core demonstrates an increased buckling load capacity of 38.37% and an enhanced energy dissipation capacity of 342.62% compared to aluminum alloy rods. Moreover, the ALECC core exhibits good hysteresis energy dissipation capability with stable hysteresis performance. The numerical analysis results validate the effectiveness of the design method and the superiority of the core structure.

Acknowledgement

Project Item: Yunjiaoke Jiaobian [2021]: No.29

References

1. Guo Y, Zhang B, Wang X, et al. (2013). Research Progress on Design Theory of Assembled Anti-buckling Supports[J]. Journal of Architecture and Civil Engineering, 30(01), 1-12. (In Chinese)
2. Zhang Y, Feng P, Dong Y, et al. (2017). Current Application Status of Anti-buckling Supports in Seismic Mitigation Systems for Bridge Engineering[J]. Earthquake Resistant Engineering and Retrofitting, 39(06), 50-55. (In Chinese)
3. Ouyang H. (2020). Research on Energy Dissipation and Seismic Reduction of Anti-buckling Restrained Supports in Reinforced Concrete Frame Structures [D]. Suzhou University of Science and Technology. (In Chinese)
4. MANABE N, SHIMOKAWA H, KAMIYA M, et al. Elasto-plastic behavior of flat-bar brace stiffened by square steel tube: Summaries of Technical Papers of Annual Meeting[C], 1996. Architectural Institute of Japan.
5. MURASE Y, MORISHITA K, INOUE K. Structural design method of the long brace with axial hysteresis dampers at both ends. Part 1: Analysis on the buckling restraint conditions[J]. Journal of Structural and Construction Engineering(Transactions of AIJ), 2004,69(578):131-138.
6. ODA H, USAMI T. Fabricating buckling-restrained braces from existing c-section bracing members: experimental study[J]. Journal of Structural Engineering, JSCE, 2010,56(A):499-510.

7. Li W, Wu B, Ding Y, et al. (2013). Experimental Study on Seismic Performance of H-shaped Steel Anti-buckling Supports[J]. Journal of Building Structures, 34(12), 94-102. (In Chinese)
8. Jin X, Han W, Cui J, et al. (2022). Calculation Method of Fatigue Life for Assembled H-shaped Steel Anti-buckling Supports[J]. Shanxi Architecture, 48(17), 58-60. (In Chinese)
9. TSAI K C, HSIAO P C. Pseudo-dynamic test of a full-scale CFT/BRB frame—Part II: Seismic performance of buckling-restrained braces and connections[J]. Earthquake Engineering & Structural Dynamics, 2008,37(7):1099-1115.
10. Deng X, Yang Y, Zhou Y, et al. (2012). Performance of New Type of Steel Reinforced Concrete Encased Steel Pipe Anti-buckling Energy Dissipation Support[J]. Journal of Chongqing Jianzhu University, 34(1), 21-28. (In Chinese)
11. TADA M, KUWAHARA S, YONEYAMA T. Horizontally loading test of the steel frame braced with double-tube members [J]. 1993.
12. Yang Y, Deng X, Qian H, et al. (2010). Performance Study of Double Steel Pipe Anti-buckling Supports[J]. Earthquake Resistant Engineering and Retrofitting, 32(2), 75-80. (In Chinese)
13. Liu L, Wu B. (2016). Analysis of Vibration Reduction Effect of Self-resetting Anti-buckling Support Steel Frame[J]. Journal of Building Structures, 37(04), 93-101. (In Chinese)
14. CHOU C, TSAI W, CHUNG P. Development and validation tests of a dual-core self-centering sandwiched buckling-restrained brace (SC-SBRB) for seismic resistance[J]. Engineering Structures, 2016,121:30-41.
15. Zhang A, Feng X, Liu X. (2017). Seismic Performance Research on H-shaped Steel Core Self-resetting Anti-buckling Supports[J]. Industrial Construction, 47(03), 25-30. (In Chinese)
16. Liu L, Wu B, Li W, et al. (2012). Quasi-static Test of a New Type of Self-resetting Anti-buckling Support[J]. Journal of Southeast University (Natural Science Edition), 42(03), 536-541. (In Chinese)
17. Hu Q. (2022) Research on the Axial Compression Mechanical Properties of High Strength Concrete Columns with Dual Constraints of Steel Tube CFRP Hoops [D]. GUANGZHOU University.
18. Peng Y, Zhao L, Li L. (2020). Mechanics of Materials [M]. Chengdu: University of Electronic Science and Technology Press. (In Chinese)
19. Long Y, Bao S. (1988). Tutorial on Structural Mechanics (Volume I) [M]. Beijing: Higher Education Press. (In Chinese)
20. Jia B, Zhang Q, Luo X. (2018). Research on Fatigue Performance of Aluminum Alloy Materials for Structural Use[J]. China Civil Engineering Journal, 51(08), 21-27. (In Chinese)
21. Li G, Yan H, Qiu Z. Hysteresis performance test of double aluminum alloy plate-assembled buckling-restrained braces[J]. Journal of Building Structures, 2023,44(05):209-220.
22. Yuan F, Pan J, Wu Y. Numerical study on flexural behaviors of steel reinforced engineered cementitious composite (ECC) and ECC/concrete composite beams[J]. Science China Technological Sciences, 2014, 57(3):637-645. (In Chinese)
23. Cheng G. (2016). Experimental Study on Mechanical Properties of Square Section Short Columns Confined by Hoop Reinforcement ECC [D]. Mechanics, Henan Polytechnic University. (In Chinese)
24. Wu K. (2017). Study on Seismic Performance of Improved Anti-buckling Supports at Ends and Energy Dissipation Mechanism of Frame Structures [D]. Kunming University of Science and Technology. (In Chinese)